Guanine quantum defects in carbon nanotubes for biosensing

*Phillip Galonska[1], Jennifer M. Mohr[1], C. Alexander Schrage[1], Lena Schnitzler[1], Sebastian Kruss[1,2]**

[1] Department of Chemistry, Ruhr University Bochum, Bochum, Germany

[2] Fraunhofer Institute for Microelectronic Circuits and Systems, Duisburg, Germany

AUTHOR INFORMATION

Corresponding Author

* Sebastian Kruss, Email: sebastian.kruss@rub.de

ABSTRACT

Fluorescent single wall carbon nanotubes (SWCNTs) are used as nanoscale biosensors in diverse applications. Selectivity is built in by non-covalent functionalization with polymers such as DNA. In general, fluorescence sensing with SWCNTs would benefit from covalent DNA-conjugation but it is not known how changes in conformational flexibility and photophysics affect the sensing mechanism. Recently, covalent functionalization was demonstrated by conjugating guanine bases of adsorbed DNA to the SWCNT surface as guanine quantum defects (g-defects). Here, we create guanine defects in $(GT)_{10}$ coated SWCNTs (G^d-SWCNTs) and explore how this affects molecular sensing. We vary the defect densities, which shifts the E_{11} fluorescence emission by 55 nm to λ_{max} = 1049 nm for the highest defect density. Furthermore, the difference between absorption maximum and emission maximum (Stokes shift) increases with increasing defect density by 0.87 nm per nm of absorption shift and up to 27 nm in total. G^d-SWCNTs represent sensitive sensors and increase their fluorescence >70 % in response to the important neurotransmitter dopamine and decrease 93 % in response to riboflavin. Additionally, cellular uptake of G^d-SWCNTs decreases. These results show how physiochemical properties alter with guanine defects and that G^d-SWCNTs constitute a versatile optical biosensor platform.

TOC GRAPHICS

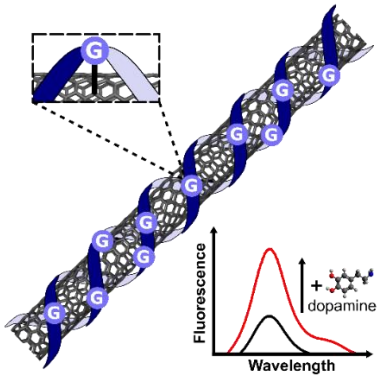

KEYWORDS

Carbon nanotubes, fluorescence, biosensors, near infrared, quantum defects, DNA, dopamine

Single wall carbon nanotubes (SWCNTs) are one-dimensional nanomaterials and can be considered as rolled-up graphene sheets. The roll-up direction is described by the chirality (n,m) and determines their properties[1]. SWCNTs of certain (n,m) chiralities are semiconductors and fluoresce in the near infrared (NIR), which falls into the tissue transparency window and provides less scattering and background signals[2,3]. The fluorescence of SWCNTs does not bleach but is highly sensitive to changes in their local environment[4,5]. These unique properties make SWCNTs ideal building blocks for biomedical sensors and various applications in this field have already been demonstrated[3,6]. Biomolecules such as the important neurotransmitters dopamine[7] or serotonin[8], riboflavin (vitamin B2)[9,10], small metabolites for pathogen identification[11], stress indicators like H_2O_2[12,13] or even peptides[14] and proteins[15–17] can be detected by SWCNT-based biosensors. Most of these sensors are designed by non-covalent surface chemistry with various kinds of polymers such as single-stranded DNA (ssDNA) or polyethylene glycols that create a corona phase around the SWCNT[3]. This organic corona phase determines selectivity and sensitivity of the sensor because it controls both molecular recognition as well as fluorescence changes[7,9]. Additionally, factors such as ion and surface accessibility or porosity have been shown to be important[18].

In the past decade, there have also been reports of covalent modification of SWCNTs. Fluorescent SWCNTs with a red-shifted NIR emission feature are generated by introducing sp^3 'quantum defects' into the sp^2 lattice of the SWCNTs[19–27]. Such quantum defects have been even used to conjugate nanobodies or even grow peptides on the SWCNT surface[28,29]. Furthermore, pH sensitive moieties[30] and boronic acid motifs[31] to bind alcohols have been demonstrated. SWCNTs modified with quantum defects can also serve as sensors but the fluorescence change was inverted to similar SWCNTs without the quantum defects[32]. More recently, Zheng *et al.* demonstrated

covalent SWCNT modification with ssDNA. Here, the dye rose Bengal (RB) is used to create singlet oxygen upon irradiation with green light. Singlet oxygen selectively reacts with guanine bases in DNA to create a guanine endo peroxide. The activated guanine attacks the sidewall of the SWCNTs and forms a covalent bond. Therefore, the dose of singlet oxygen and the guanine content of the ssDNA sequence determine the number of guanines bound to the SWCNT surface. The singlet oxygen dose is adjusted by the SWCNT/RB ratio in the reaction solution, as the RB reaction is irreversible[33–36]. In contrast to sp^3 defects, guanine defects (g-defects) are considered to create sp^2 hybridized carbons[37]. The wave functions of the defects overlap as a consequence of spatial proximity between g-defects and create more shallow exciton traps. Unlike sp^3 defect SWCNTs, guanine defect functionalized SWCNTs (G^d-SWCNTs) only have a single NIR emission feature, which is redshifted and broadened compared to pristine SWCNTs. This surface chemistry enables also well-defined and periodic DNA structures around SWCNTs[37]. So far it is not understood if covalent binding of DNA to the SWCNT surface affects the sensing mechanism in DNA-SWCNT-based biosensors.

SWCNTs are versatile sensors, which are frequently used in biological environments *in vitro* and *in vivo*. The interaction of a SWCNT with a cellular membrane and therefore the transportation process across the membrane depends on the SWCNT´s surface properties such as size or charge. Until now, both passive and active uptake mechanism of SWCNTs into cells over the cell membrane have been described. Most data suggest an energy dependent uptake of SWCNTs into the cell via clathrin-dependent endocytosis[38]. In contrast, in energy independent uptake (nano-penetration) SWCNTs move through the cell membrane into the cytosol[39].

In this work, we explore G^d-SWCNTs for biosensing applications. To use G^d-SWCNTs in sensing applications, a surfactant-free synthesis of g-defects is required as already small amounts of surfactant are sufficient to disturb the sensing mechanisms in DNA-SWCNT sensors[40].

For this purpose, $(GT)_{10}$-ssDNA functionalized SWCNTs were exposed to RB and light in aqueous phosphate buffered saline (PBS). The reaction solution was next dialyzed against PBS to remove residual RB. The complete removal of the chromophore RB from the sample was verified by absorption spectroscopy[41]. In agreement with the literature[35], defect introduction caused a bathochromic shift and broadened the E_{11} NIR fluorescence feature (Figure 1 a, b). DNA-SWCNTs illuminated in presence of higher RB concentrations had higher defect densities and hence stronger bathochromic shifts and peak-broadening. Next, we wanted to know if the amount of DNA, which is only loosely bound and can be removed from the SWCNTs changes for this covalent chemistry. Therefore, the product of the reaction was washed by spin filtration and the DNA amount in the washing solution was measured by absorption spectroscopy[42]. First, PBS buffer was used to remove free DNA from the solution. It is expected, that adsorbed DNA will not be affected by this process. Surface adsorbed DNA was removed from the SWCNTs in a second step by washing with the surfactant sodium cholate (SC), which occupies the SWCNT surface and removes non-covalently bound DNA[43,44]. For PBS washing steps, the amount of removable DNA decreased with increasing defect density. For washing with SC no significant difference was visible for different defect densities (Figure S1). Therefore, for G^d-SWCNTs more DNA-molecules are strongly bound than for pristine SWCNTs. To test the influence of the covalent character of surface functionalization on analyte recognition, 100 µM dopamine (DA) or riboflavin were added to G^d-SWCNTs of different defect densities (Figure 1 c, d, S2). To compare defect densities between sensors, the position of the E_{11} peak was compared. All sensors showed a strong

fluorescence increase upon dopamine addition. Fluorescence of pristine SWCNTs increased by 113 % whereas fluorescence of G^d-SWCNTs with a high defect density (G^d_{high}-SWCNTs) increased by 72 % (Figure 1 d).

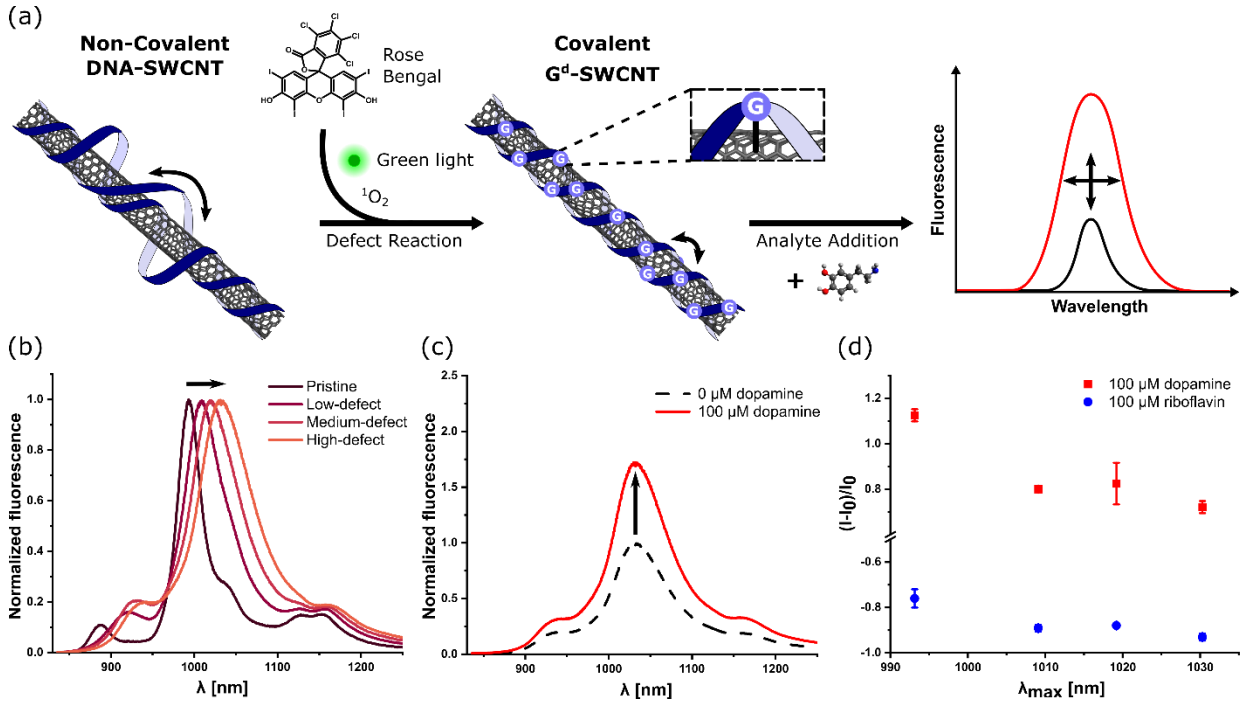

Figure 1: Fluorescence-based sensing with guanin defect-SWCNTs. *(a) Schematic of synthesis and potential applications of G^d-SWCNTs as sensors. Here, the nomenclature G^d indicates that the guanine bases are covalently bound to the SWCNT lattice. (b) NIR-fluorescence spectra of $(GT)_{10}$-SWCNTs of increasing g-defect densities. (c) NIR-fluorescence spectra of high-defect G^d-SWCNTs before (black, dashed) and after (red) addition of 100 µM dopamine shows that they act as sensors. (d) Relative fluorescence changes after addition of different analytes that increase (dopamine) or decrease (riboflavin) fluorescence. Note that the E_{11} peak position (x-axis) is a measure for defect density. Error bars are standard deviations (n = 3).*

In contrast to DA, riboflavin quenches SWCNT fluorescence[9]. Fluorescence of pristine SWCNTs decreased by 76 % in response to riboflavin (100 µM) and G^d_{high}-SWCNTs fluorescence decreased by 93 %. Hence, the riboflavin response was stronger for G^d-SWCNTs than for pristine SWCNTs, which was opposite as for dopamine. To describe the fluorescence modulation in DNA-SWCNTs, many models have been discussed[3,45]. One prominent model assumes a change in the DNA conformation, induced by the formation of bonds between the hydroxy groups of dopamine and the phosphate backbone of the DNA[7]. A side effect of the covalently bound DNA in G^d-SWCNTs could be a smaller degree of conformational freedom of the corona phase. Flexibility of the corona phase is expected to correlate inversely with defect density. The limited ability of the corona phase to change its conformation could therefore decrease the sensor response. The fact that the sensor response of G^d-SWCNTs depends on defect density, with the lowest response occurring at the greatest defect density (Figure 1 d) supports this hypothesis for dopamine. Riboflavin, on the other hand, quenched G^d-SWCNTs more efficiently, but the difference in sensor responses of pristine and G^d-SWCNTs was smaller. These different patterns suggest different sensing mechanisms. One explanation could be that for riboflavin the redox properties and the related optical properties play a role[9].

Next, binding affinities of G^d-SWCNTs were compared to pristine sensors. For this purpose, dopamine dose-response curves for pristine, low- and high-defect SWCNTs were recorded (Figure 2 a). Pristine SWCNTs reached saturation at a concentration of 10 µM with a maximum fluorescence increase of 129 %, whereas G^d-SWCNTs already saturated at 1 µM dopamine. The lower saturation is also reflected in a slightly different K_D value obtained from the sigmoidal fit. For pristine SWCNTs $K_D = 62 \pm 7$ nM was obtained. SWCNTs of low defect density showed

K_D = 21 ± 9 nM and SWCNTs of high defect density K_D = 35 ± 30 nM. The marginally lower K_D found in G^d-SWCNTs can be attributed to the more rigid DNA-corona, offering less conformational freedom in response to dopamine DNA/SWCNT interactions. RB is an organic dye and therefore expected to quench SWCNT fluorescence[46]. Indeed, already low concentrations of RB strongly quenched the fluorescence of SWCNTs (Figure 2 b, c). Quenching correlated with defect density and G^d-SWCNTs were quenched less than pristine SWCNTs. Upon addition of dopamine, pristine SWCNTs quenched by RB increased their fluorescence by up to 3100 % (Figure 2 d). In contrast to sensitivity, sensor selectivity was not affected by g-defects. Indeed, the fluorescence responses of G^d-SWCNTs to the homologues epinephrine, norepinephrine and the interfering substance ascorbic acid were not affected by defect density (Figure S3). In accordance with the slightly decreased dopamine response in G^d-SWCNTs, the less flexible corona makes SWCNTs also more robust against RB induced fluorescence quenching (Figure 2 c). The strong influence of only small amounts of RB emphasizes the importance of careful sample purification in the surfactant-free g-defect synthesis protocol. On the other hand, RB-quenched SWCNTS provide an interesting platform for the design of SWCNT based turn-on sensors. The extreme fluorescence increase observed here is most likely a displacement of RB by dopamine from the hydrophobic SWCNT surface. Hereby, the SWCNT is turned from a nearly dark (RB-quenched) state into a bright (dopamine induced) state.

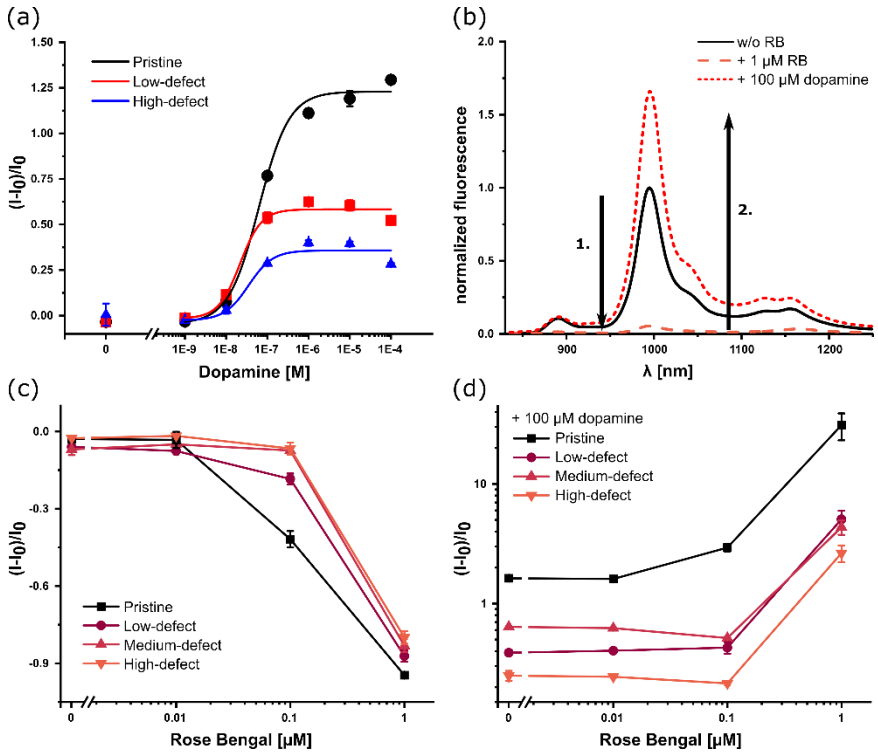

Figure 2: Sensing characteristics of G^d-SWCNTs*. (a) Dose response curve of SWCNTs with different defect densities for the neurotransmitter dopamine. Lines are sigmoidal fits (Hill function). (b) Normalized fluorescence spectra of pristine SWCNTs before addition of RB, after RB addition (1.) and after addition of both RB and dopamine (2.) show the strong impact of RB on SWCNT fluorescence and sensing. (c) RB quenches fluorescence of pristine and G^d-SWCNTs. (d) Fluorescence response of SWCNTs to 100 µM dopamine in presence of RB is higher for non-covalently modified SWCNTs. Error bars are standard deviations (n = 3).*

For *in vivo* applications of sensors the light should be able to reach also deeper tissue levels[3,6]. In pristine SWCNTs excitation and emission nearly completely overlap in the NIR (Stokes shift < 2 nm). Such a small Stokes shift means that it is difficult to separate excitation and emission light efficiently. Interestingly, we find that the Stokes shift in G^d-SWCNTs linearly increases with the

peak position of fluorescence (Figure 3). The linear fit shows that for each nanometer shift in absorption peak position the Stokes shift is increased by 0.87 $nm_{emission}/nm_{absorbance}$ leading to a maximum Stokes shift of 27.5 nm for G^d_{high}-SWCNTs. This is in agreement with a correlation between peak broadening in G^d-SWCNTs and fluorescence emission redshift[37]. The large Stokes shift in G^d_{high}-SWCNTs allows both excitation and emission readout in the beneficial NIR-tissue transparency window. This promises even deeper tissue penetration and makes g-defects useful for *in vivo* application of SWCNTs. The extended Stokes shift can be considered as a consequence of elongated exciton lifetimes in the shallow g-defect traps[35], leading to a loss of energy due to local interactions[32,47].

The availability of covalent surface chemistry for DNA-SWCNT sensors promises increased robustness in complex environments allowing more sophisticated applications in biological systems[33].

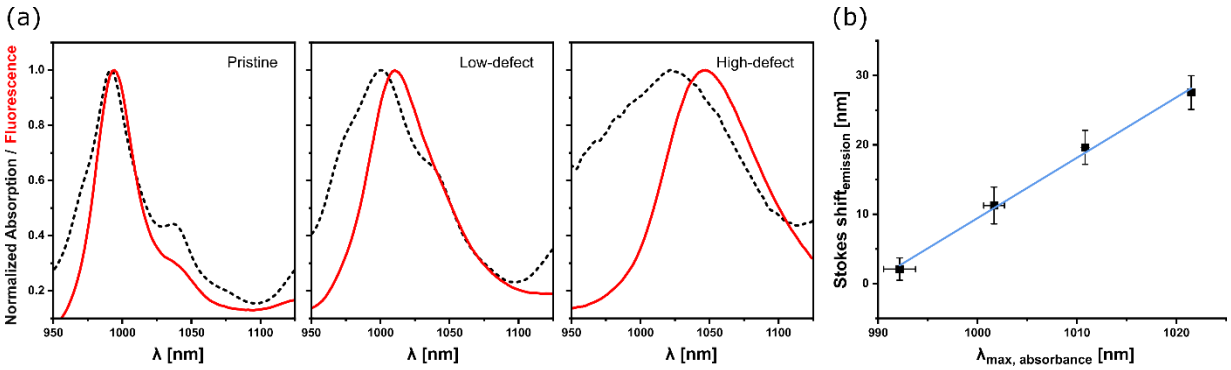

Figure 3: Stokes shift of G^d-SWCNTs increases with defect density. *(a) Normalized absorption and fluorescence spectra of pristine, low- and high defect density $(GT)_{10}$-SWCNTs (from left to right). (b) Stokes shift between absorption and emission of $(GT)_{10}$-SWCNTs for different defect densities. Both spectra red-shift with increasing defect density but the fluorescence shifts more. The blue line is a linear regression fit ($R^2 = 0.994$) with $m = 0.87 \pm 0.04$. Error bars are standard deviations (n=3).*

Next, we wanted to find out how G^d-SWCNTs perform in cellular environments. Incubation of SWCNTs in cell culture medium (see materials section) led to a significant change in fluorescence intensity in pristine SWCNTs whereas the change in G^d-SWCNTs fluorescence intensity change was very low (Figure S4). This indicates increased stability in such complex environments. It is also interesting to study if the change in DNA flexibility affects the interaction with cells e,g. the cell membrane. For DNA-SWCNTs it is known that they are able to pass cell membranes and accumulate inside the cells[48–52]. Depending on the intended application, this is either wanted (gene delivery) or a problem (extracellular sensing). To test if membrane interaction of DNA-SWCNTs is changed by g-defects, we incubated HeLa cells for one hour with 1 nM SWCNT solutions of

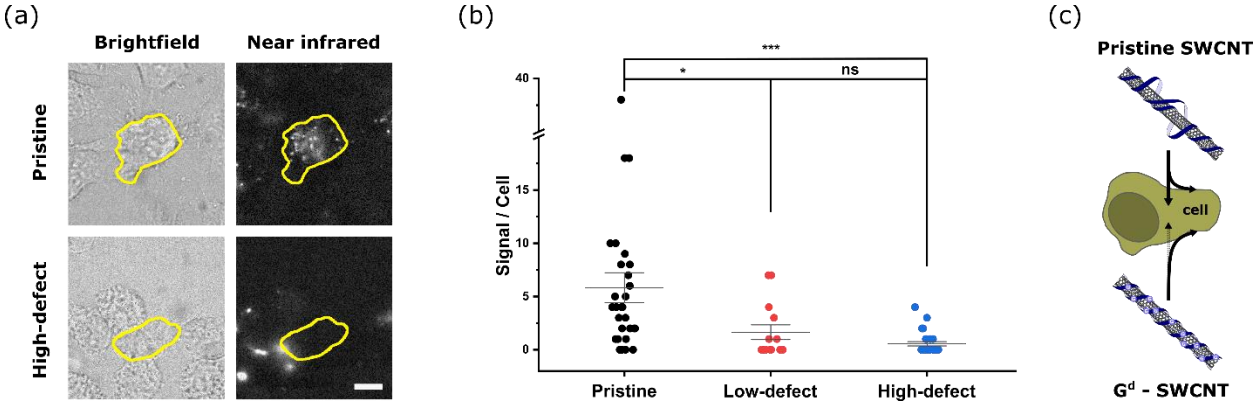

Figure 4: Interactions of G^d-SWCNTs with cells*. (a) Brightfield and near infrared images (> 900 nm) of HeLa cells incubated with SWCNTs of different defect densities. G^d-SWCNTs interact to a certain extent with the cells and adsorb to the cell surface but the number of single SWCNT signals inside the cells is lower. Scale bar = 10 µm. (b) NIR signal intensities (single resolution limited spots of SWCNTs) per cels for pristine versus G^d-SWCNTs of different defect densities indicate different uptake. Mean ± standard error is depicted. Statistics: Two sample t-test. ***: $p < 0.005$, *: $p < 0.05$, ns: non-significant. (c) Schematic of altered cell uptake of G^d-SWCNTs by cells.*

different defect densities in Iscove's Modified Dulbecco's Medium (IMDM) with 10 % fetal calf serum (FCS) and 1 % Penicillin-Streptomycin (P/S).

After incubation, the cells were washed with IMDM to remove free SWCNTs in solution and imaged in a NIR fluorescence microscopy setup to localize single SWCNTs. This incubation protocol is consistent with the paint methodology recently used for dopamine detection (AndromeDA).[53] We found strong single NIR-fluorescence signals inside cells incubated with pristine SWCNTs. For cells incubated with G^d-SWCNTs, NIR fluorescence colocalized rather with the cell membranes than with the cytosol (Figure 4 a). This observation was quantified by comparing the SWCNT signals and the boundaries outer membranes of healthy cells from the brightfield image and automated identification[54] of SWCNT signals inside the cell. Indeed, G^d-SWCNTs were found significantly fewer inside cells than pristine SWCNTs (Figure 4 b). These results show that the uptake probability decreases and membrane passage is affected by the covalent chemistry. For applications of SWCNTs e.g. as sensors it is desirable to have precise control of the interaction between them and the biological system. The altered cellular uptake observed in G^d-SWCNTs is such a control mechanism and allows to influence localization of SWCNTs more precisely. G^d-SWCNT applications in biological contexts, e.g. for neurotransmitter detection[3,8,55] or as cellular delivery vehicles[48,56–59] could profit from this additional layer of control. Our studies leave it open whether an active or inactive uptake mechanism is affected by g-defects[48]. In some cases, G^d-SWCNTs were still able to enter cells. Therefore, it is likely that not all mechanisms are affected and physisorption onto the outer cell membrane still takes place.

In summary, we demonstrated surfactant free covalent DNA chemistry on SWCNTs to create fluorescent biosensors. The covalently functionalized SWCNTs retain their sensitivity to prominent targets such as dopamine or riboflavin. The reduced flexibility of DNA in G^d-SWCNTs

provides new insights into the molecular recognition mechanism of the sensors. It underlines the importance of corona conformational changes as mechanism of fluorescence changes. Furthermore, the covalent chemistry affects the fate of DNA-SWCNTs in biological systems. With increasing defect density, G^d-SWCNTs are taken up less by cells and remain on the outside of the membrane. In addition to the advantages of covalent chemistry the photophysical properties of SWCNTs are altered. The density of g-defects enables precise tailoring of the absorption and fluorescence wavelengths of SWCNTs, promising all NIR imaging for biological applications. Overall, g-defects are a powerful tool to alter and tailor SWCNT-based sensors and promise new versatile sensor designs.

EXPERIMENTAL METHODS

Nanotube Functionalization

To disperse SWCNTs in DNA, 0.5 ml of 2 mg/ml CoMoCAT SWCNTs (Merck, product no. 773735) in 1 x PBS (Roth, product no. 9143.2) was mixed with 1 ml of 2 mg/ml $(GT)_{10}$-ssDNA (oligos ordered from Merck) in 1 x PBS. The mixture was placed in a tip-sonicator (Fischer Scientific model 120 Sonic Dismembrator) and sonicated for 40 minutes at 45 % amplitude (72 W output power, pulsed) in an ice-water bath. After sonication the sample was centrifuged at 21,000 g for 30 minutes. The supernatant was transferred to a new vial and the procedure was repeated two more times. Sample concentration was determined by absorption spectroscopy (Jasco V-770 UV-Visible/NIR Spectrophotometer) from 400 to 1350 nm with 0.5 nm steps in a 10 mm path polystyrene cuvette (Sarstedt, product no. 67.742). From full width at half maximum (FWHM) and maximum fluorescence intensity of the E_{11} absorption feature of (6,5)-SWCNTs the concentration was determined. Here, an oscillator strength of $f_c = 0.01$ and 52,800 carbon atoms per SWCNT (for a 600 nm long SWCNT) were assumed[42,60].

Defect Reaction

Guanine defects were created by mixing 10 nM DNA-functionalized SWCNTs with the respective concentrations of RB (Merck, product no. 198250) to a total volume of 2 ml and irradiation at 561 nm under stirring for 15 min in a custom build light chamber. After defect introduction, the sample was dialyzed against 500 ml 1 x PBS for at least four days in a 300 kDa dialysis bag (Spectra/Por, product no. 131450) and daily buffer exchange. Concentration was determined by absorption spectroscopy as mentioned above. The success of defect reactions could be followed by bathochromic shifts of the E_{11} absorption maximum and increased FWHM. Residual RB could be detected (if present) at around 560 nm in the absorption spectrum.

Fluorescence Spectroscopy

For fluorescence spectroscopy 198 µl sample solution was placed in a 96 well plate. For analyte sensing, 2 µl of the analyte was added to the sample solution. The well plate was placed on an IX73 microscope (Olympus) and fluorescence spectra were acquired by a Shamrock193i spectrometer (Andor Technology Ltd.), connected to the microscope. Sample excitation was performed using a gem 561 nm laser (Laser Quantum) at 100 mW excitation power.

Fluorescence Imaging

For imaging a custom-built setup was used. A 561 nm laser for NIR fluorescence excitation (Cobolt Jive^{TM}) was coupled into an Olympus IX73 microscope equipped with a 100× (UPlanSApo 100×/1.35 Sil, Olympus) oil immersion objective. NIR and brightfield could simultaneously be imaged. For NIR imaging a Xenics Cheetah TE1 InGaAs camera was used. A dichroic mirror (VIS/NIR, HC BS R785 lambda/5 PV, F38-785, AHF) and a 900 nm long-pass

filter (FELH0900, Thorlabs) were installed in the beam path between objective and cameras. NIR images where acquired with 60 mW excitation laser power at 1 fps (0.9 s exposure time). Cells were seeded into 96 glass-bottom well plates (P96-0-N, Cellvis) which were placed on the microscope. Temperature was kept constant at 37 °C by placing an incubation chamber (Tokai Hit STXG-DMIWX) on top of the well plate on the microscope.

Cell-culture

Cells were derived from cervical cancer (HeLa cell line). They were cultured in Iscove´s Modified Dulbecco´s Medium (IMDM) with 10 % fetal calf serum (FCS) and 1 % Penicillin-Streptomycin (P/S). Cells were seeded one day prior to microscopy at 20 000 cells per 96 well glass bottom chamber with 200 µl IMDM Medium with 10 % FCS and 1 % P/S in each well. For this purpose, the cells were detached from the cell culture dish with Trypsin/EDTA, counted and then seeded accordingly. The next day the functionalized SWCNTs were directly added to the wells into the medium resulting in a final concentration of 1 nM. After 1 h incubation the cells were washed three times with IMDM with 10 % FCS and 1 % P/S and imaged in the same medium.

AUTHOR INFORMATION

The authors declare no competing financial interests.

ACKNOWLEDGMENT

This work was supported by RESOLV, funded by the Deutsche Forschungs-Gemeinschaft (DFG, German Research Foundation) under Germany's Excellence Strategy—EXC-2033—project number 3906778. Furthermore, this work is supported by the „Center for Solvation Science ZEMOS" funded by the German Federal Ministry of Education and Research BMBF and by the Ministry of Culture and Research of Nord Rhine-Westphalia.

SUPPLEMENTARY INFORMATION AVAILABLE

Additional fluorescence spectra and plots for surface-DNA quantification, selectivity and stability experiments (PDF).

REFERENCES

1. Bachilo, S. M. *et al.* Structure-assigned optical spectra of single-walled carbon nanotubes. *Science* **298**, 2361–2366 (2002).

2. Hong, G., Antaris, A. L. & Dai, H. Near-infrared fluorophores for biomedical imaging. *Nat. Biomed. Eng.* **1**, (2017).

3. Ackermann, J., Metternich, J. T., Herbertz, S. & Kruss, S. Biosensing with Fluorescent Carbon Nanotubes. *Angew. Chemie Int. Ed.* **202112372**, (2022).

4. O'Connell, M. J. *et al.* Band gap fluorescence from individual single-walled carbon nanotubes. *Science* **297**, 593–596 (2002).

5. Cognet, L. *et al.* Stepwise quenching of exciton fluorescence in carbon nanotubes by single-molecule reactions. *Science* **316**, 1465–1468 (2007).

6. Hong, G., Diao, S., Antaris, A. L. & Dai, H. Carbon Nanomaterials for Biological Imaging and Nanomedicinal Therapy. *Chem. Rev.* **115**, 10816–10906 (2015).

7. Kruss, S. *et al.* Neurotransmitter detection using corona phase molecular recognition on fluorescent single-walled carbon nanotube sensors. *J. Am. Chem. Soc.* **136**, 713–724 (2014).

8. Dinarvand, M. *et al.* Near-Infrared Imaging of Serotonin Release from Cells with Fluorescent Nanosensors. *Nano Lett.* **19**, (2019).

9. Polo, E. & Kruss, S. Impact of Redox-Active Molecules on the Fluorescence of Polymer-Wrapped Carbon Nanotubes. *J. Phys. Chem. C* **120**, 3061–3070 (2016).

10. Zhang, J. *et al.* Molecular recognition using corona phase complexes made of synthetic

polymers adsorbed on carbon nanotubes. *Nat. Nanotechnol.* **8**, 959–968 (2013).

11. Nißler, R. *et al.* Remote near infrared identification of pathogens with multiplexed nanosensors. *Nat. Commun.* **11**, 1–12 (2020).

12. Wu, H. *et al.* Monitoring Plant Health with Near-Infrared Fluorescent H2O2 Nanosensors. *Nano Lett.* **20**, 2432–2442 (2020).

13. Safaee, M. M., Gravely, M. & Roxbury, D. A Wearable Optical Microfibrous Biomaterial with Encapsulated Nanosensors Enables Wireless Monitoring of Oxidative Stress. *Adv. Funct. Mater.* **31**, (2021).

14. Ehrlich, R., Hendler-Neumark, A., Wulf, V., Amir, D. & Bisker, G. Optical Nanosensors for Real-Time Feedback on Insulin Secretion by β-Cells. *Small* **17**, 2101660 (2021).

15. Budhathoki-Uprety, J. *et al.* Synthetic molecular recognition nanosensor paint for microalbuminuria. *Nature Communications* vol. 10 (2019).

16. Bisker, G. *et al.* Protein-targeted corona phase molecular recognition. *Nat. Commun.* **7**, 1–14 (2016).

17. Xu, X. *et al.* Tuning Electrostatic Gating of Semiconducting Carbon Nanotubes by Controlling Protein Orientation in Biosensing Devices. *Angewandte Chemie - International Edition* vol. 60 20184–20189 (2021).

18. Gillen, A. J. *et al.* Templating colloidal sieves for tuning nanotube surface interactions and optical sensor responses. *J. Colloid Interface Sci.* **565**, 55–62 (2020).

19. Ghosh, S., Bachilo, S. M., Simonette, R. A., Beckingham, K. M. & Weisman, R. B. Oxygen

doping modifies near-infrared band gaps in fluorescent single-walled carbon nanotubes. *Science* **330**, 1656–1659 (2010).

20. Piao, Y. *et al.* Brightening of carbon nanotube photoluminescence through the incorporation of sp3 defects. *Nat. Chem.* **5**, 840–845 (2013).

21. Kwon, H. *et al.* Molecularly Tunable Fluorescent Quantum Defects. *J. Am. Chem. Soc.* **138**, 6878–6885 (2016).

22. Miyauchi, Y. *et al.* Brightening of excitons in carbon nanotubes on dimensionality modification. *Nat. Photonics* **7**, 715–719 (2013).

23. Kim, M. *et al.* Mapping Structure-Property Relationships of Organic Color Centers. *Chem* **4**, 2180–2191 (2018).

24. Godin, A. G. *et al.* Photoswitchable single-walled carbon nanotubes for super-resolution microscopy in the near-infrared. *Sci. Adv.* **5**, eaax1166 (2019).

25. Chiu, C. F., Saidi, W. A., Kagan, V. E. & Star, A. Defect-Induced Near-Infrared Photoluminescence of Single-Walled Carbon Nanotubes Treated with Polyunsaturated Fatty Acids. *J. Am. Chem. Soc.* **139**, 4859–4865 (2017).

26. Janas, D. Perfectly imperfect: A review of chemical tools for exciton engineering in single-walled carbon nanotubes. *Materials Horizons* vol. 7 2860–2881 (2020).

27. Wang, H. & Boghossian, A. A. Covalent conjugation of proteins onto fluorescent single-walled carbon nanotubes for biological and medical applications. *Mater. Adv.* 823–834 (2022) doi:10.1039/d2ma00714b.

28. Mann, F. A., Herrmann, N., Opazo, F. & Kruss, S. Quantum Defects as a Toolbox for the Covalent Functionalization of Carbon Nanotubes with Peptides and Proteins. *Angew. Chemie - Int. Ed.* **59**, 17732–17738 (2020).

29. Mann, F. A., Galonska, P., Herrmann, N. & Kruss, S. Quantum defects as versatile anchors for carbon nanotube functionalization. *Nat. Protoc.* (2022) doi:10.1038/s41596-021-00663-6.

30. Kwon, H. *et al.* Optical Probing of Local pH and Temperature in Complex Fluids with Covalently Functionalized, Semiconducting Carbon Nanotubes. *J. Phys. Chem. C* **119**, 3733–3739 (2015).

31. Shiraki, T., Onitsuka, H., Shiraishi, T. & Nakashima, N. Near infrared photoluminescence modulation of single-walled carbon nanotubes based on a molecular recognition approach. *Chem. Commun.* **52**, 12972–12975 (2016).

32. Spreinat, A. *et al.* Quantum Defects in Fluorescent Carbon Nanotubes for Sensing and Mechanistic Studies. *J. Phys. Chem. C* **125**, 18341–18351 (2021).

33. Zheng, Y., Bachilo, S. M. & Weisman, R. B. Controlled Patterning of Carbon Nanotube Energy Levels by Covalent DNA Functionalization. *ACS Nano* (2019) doi:10.1021/acsnano.9b03488.

34. Zheng, Y. *et al.* Quantum Light Emission from Coupled Defect States in DNA-Functionalized Carbon Nanotubes. *ACS Nano* **15**, 10406–10414 (2021).

35. Zheng, Y. *et al.* Photoluminescence Dynamics Defined by Exciton Trapping Potential of Coupled Defect States in DNA-Functionalized Carbon Nanotubes. *ACS Nano* **15**, 923–933

(2021).

36. Zheng, Y., Alizadehmojarad, A. A., Bachilo, S. M. & Weisman, R. B. Guanine-Specific Chemical Reaction Reveals ssDNA Interactions on Carbon Nanotube Surfaces. *J. Phys. Chem. Lett.* **13**, 2231–2236 (2022).

37. Lin, Z. *et al.* DNA-guided lattice remodeling of carbon nanotubes. *Science* **377**, 535–539 (2022).

38. Kam, N. W. S., Liu, Z. & Dai, H. Carbon nanotubes as intracellular transporters for proteins and DNA: An investigation of the uptake mechanism and pathway. *Angewandte Chemie - International Edition* vol. 45 577–581 (2006).

39. Jena, P. V. *et al.* Hyperspectral Counting of Multiplexed Nanoparticle Emitters in Single Cells and Organelles. *ACS Nano* **16**, 3092–3104 (2022).

40. Nißler, R. *et al.* Sensing with Chirality-Pure Near-Infrared Fluorescent Carbon Nanotubes. (2021) doi:10.1021/acs.analchem.1c00168.

41. Rauf, M. A., Graham, J. P., Bukallah, S. B. & Al-Saedi, M. A. S. Solvatochromic behavior on the absorption and fluorescence spectra of Rose Bengal dye in various solvents. *Spectrochim. Acta - Part A Mol. Biomol. Spectrosc.* **72**, 133–137 (2009).

42. Nißler, R. *et al.* Quantification of the Number of Adsorbed DNA Molecules on Single-Walled Carbon Nanotubes. *J. Phys. Chem. C* **123**, 4837–4847 (2019).

43. Bergler, F. F., Schöppler, F., Brunecker, F. K., Hailman, M. & Hertel, T. Fluorescence spectroscopy of gel-immobilized single-wall carbon nanotubes with microfluidic control of the surfactant environment. *J. Phys. Chem. C* **117**, 13318–13323 (2013).

44. Yang, Y., Sharma, A., Noetinger, G., Zheng, M. & Jagota, A. Pathway-Dependent Structures of DNA-Wrapped Carbon Nanotubes: Direct Sonication vs Surfactant/DNA Exchange. *J. Phys. Chem. C* **124**, 9045–9055 (2020).

45. Zhang, J. *et al.* Single molecule detection of nitric oxide enabled by d(AT)15 DNA adsorbed to near infrared fluorescent single-walled carbon nanotubes. *J. Am. Chem. Soc.* **133**, 567–581 (2011).

46. Yang, R. *et al.* Carbon nanotube-quenched fluorescent oligonucleotides: Probes that fluoresce upon hybridization. *J. Am. Chem. Soc.* **130**, 8351–8358 (2008).

47. Silvera-Batista, C. A., Wang, R. K., Weinberg, P. & Ziegler, K. J. Solvatochromic shifts of single-walled carbon nanotubes in nonpolar microenvironments. *Phys. Chem. Chem. Phys.* **12**, 6990–6998 (2010).

48. Bhattacharya, S., Roxbury, D., Gong, X., Mukhopadhyay, D. & Jagota, A. DNA conjugated SWCNTs enter endothelial cells via Rac1 mediated macropinocytosis. *Nano Lett.* **12**, 1826–1830 (2012).

49. Gravely, M. & Roxbury, D. Multispectral Fingerprinting Resolves Dynamics of Nanomaterial Trafficking in Primary Endothelial Cells. *ACS Nano* **15**, 12388–12404 (2021).

50. Jin, H., Heller, D. A., Sharma, R. & Strano, M. S. Size-dependent cellular uptake and expulsion of single-walled carbon nanotubes: Single particle tracking and a generic uptake model for nanoparticles. *ACS Nano* **3**, 149–158 (2009).

51. Hermanson, G. T. *Microparticles and Nanoparticles*. *Bioconjugate Techniques* (2013).

doi:10.1016/b978-0-12-382239-0.00014-5.

52. Jin, H., Heller, D. A. & Strano, M. S. Single-particle tracking of endocytosis and exocytosis of single-walled carbon nanotubes in NIH-3T3 cells. *Nano Lett.* **8**, 1577–1585 (2008).

53. Elizarova, S. *et al.* A fluorescent nanosensor paint detects dopamine release at axonal varicosities with high spatiotemporal resolution. *Proc. Natl. Acad. Sci. U. S. A.* **119**, 1–12 (2022).

54. Ershov, D. *et al.* TrackMate 7: integrating state-of-the-art segmentation algorithms into tracking pipelines. *Nat. Methods* **19**, 829–832 (2022).

55. Kruss, S. *et al.* High-resolution imaging of cellular dopamine efflux using a fluorescent nanosensor array. *Proc. Natl. Acad. Sci.* **114**, 1789–1794 (2017).

56. Pantarotto, D. *et al.* Functionalized carbon nanotubes for plasmid DNA gene delivery. *Angew. Chemie - Int. Ed.* **43**, 5242–5246 (2004).

57. Demirer, G. S., Zhang, H., Goh, N. S., González-Grandío, E. & Landry, M. P. Carbon nanotube–mediated DNA delivery without transgene integration in intact plants. *Nat. Protoc.* **14**, 2954–2971 (2019).

58. Costa, P. M., Bourgognon, M., Wang, J. T. W. & Al-Jamal, K. T. Functionalized carbon nanotubes: From intracellular uptake and cell-related toxicity to systemic brain delivery. *J. Control. Release* **241**, 200–219 (2016).

59. Meyer, D. *et al.* Transport and programmed release of nanoscale cargo from cells by using NETosis. *Nanoscale* vol. 12 9104–9115 (2020).

60. Schöppler, F. *et al.* Molar extinction coefficient of single-wall carbon nanotubes. *J. Phys. Chem. C* **115**, 14682–14686 (2011).